Structure of a Luminescent MOF-2 Derivative with a Core of Zn(II)-Terephthalate-Isoquinoline and Its Application in Sensing of Xylenes

Luis D. Rosales-Vázquez [1], **Iván J. Bazany Rodríguez** [1], **Simón Hernández-Ortega** [1] [iD],
Víctor Sánchez-Mendieta [2,*] [iD], **Alfredo R. Vilchis-Nestor** [2] [iD], **José de Jesús Cázares-Marinero** [3]
and **Alejandro Dorazco-González** [1,*] [iD]

[1] Instituto de Química, Universidad Nacional Autónoma de México, Circuito Exterior, Ciudad Universitaria, Ciudad de México 04510, Mexico; ld_222@hotmail.com (L.D.R.-V.); ivanbazany@comunidad.unam.mx (I.J.B.R.); simonho@unam.mx (S.H.-O.)

[2] Centro Conjunto de Investigación en Química Sustentable UAEM-UNAM, Carretera Toluca-Ixtlahuaca Km. 14.5, Tlachaloya, Toluca, Estado de México 50200, Mexico; arvilchisn@uaemex.mx

[3] Departamento de Investigación y Desarrollo, Polioles S.A. de C.V. Km. 52.5 Parque Industrial Lerma, Estado de México 52000, Mexico; jose.cazares@polioles.com.mx

* Correspondence: vsanchezm@aemex.mx (V.S.M.); adg@unam.mx (A.D.G.)

check for updates

Abstract: A new blue photoluminescent 2D metal–organic framework, **1**, with formula $\{[Zn_2(\mu_2\text{-BDC})_2(iQ)_2]\}_\infty$ has been synthesized in a high yield under solvothermal conditions by reacting Zn(II) ions with 1,4-benzenedicarboxylic acid (H$_2$BDC) and isoquinoline (*i*Q) in DMF. Compound **1** was thoroughly characterized by single-crystal X-ray diffraction, solid-state cross-polarization magic-angle spinning ^{13}C NMR, X-ray powder diffraction, scanning electron microscopy (SEM) with energy dispersive X-ray spectroscopy (EDS), and thermoanalysis. The crystal structure of **1** showed interpenetrated 2D frameworks consisting of dinuclear paddle-wheel cores Zn$_2$; moreover, this material possessed thermostability up to 310 °C. The CPMAS ^{13}C-NMR spectrum of **1** is consistent with the symmetry of the crystal structure. Luminescence studies showed that **1** strongly enhances its fluorescence emission in the presence of xylene isomers with a pronounced selectivity to p-xylene.

Keywords: MOF-2 derivative; fluorescent sensing; xylene isomers

1. Introduction

There is a growing interest in the development of photoluminescent metal–organic materials (MOMs) [1–4], where the color emission upon excitation is a significant feature of these materials that has been recently used in several applications such as emitting devices/materials [5,6], optical sensing of vapor phase analytes [3,7], detection of ions [8,9], bioanalytes [10], explosives [11,12], and detection of volatile organic solvents (VOCs) [8,13,14]. Most known MOMs-based chemosensors for organic solvents act in a "turn-off" response where the fluorescence intensity of the compound is quenched upon addition of the analyte [7,15,16]. The photoluminescent properties of MOMs are basically dependent on the used metal center, its coordination environment, the presence of aromatic ligands, as well as the supramolecular interactions such as π–π stacking in the final arrangement [1]. From a synthetic point view, the combination of divalent d^{10} transition metal ions with rigid aromatic dicarboxylic acids and auxiliary *N*-donor ligands such as pyridines [17], imidazole groups [18], and isoquinline rings [19] can be used to obtain crystalline metal–organic structures with adjustable emission properties. In this context, the planar symmetric 1,4-benzenedicarboxylate (BDC) anion is a very common bridging

ligand to achieve microporous MOF-2 derivatives [20] with rigid dinuclear cores, owing to this dianion generating paddle-wheel secondary building units (SBUs) of type $[M_2(-COO)_4]$, particularly with Zn(II) ions [20–25]. In the area of optical sensing, MOMs with polynuclear d^{10} metal cores containing coordinated fluorescent ligands are very attractive because they exhibit striking crystal structures and outstanding photoluminescence properties mainly caused by charge transfer mechanisms [1,2,17,18,26].

On the other hand, methyl-substituted aromatic VOCs such as the xylene isomers and toluene are usually used as organic solvents in the industrial production of adhesives, rubber products, dyes, and paints [27]. Among these isomers, p-xylene is the most used in the industry mainly in the production of polyesters [28]. They are carcinogenic species and considered as some of the most hazardous pollutants among VOCs [29]. Acute exposure to xylene isomers and toluene, typically found in gasoline, has been associated with skin, eye irritation, and effects on the respiratory system [30]. The constant and chronic exposure to small amounts of these solvents (200 ppm or greater) in the ambient or at home with common products such as adhesives and solvents for paints is associated with various adverse health effects [27,31]. Data on the xylene isomers concentration in these products used at home or work are usually incomplete. While the need for rapid quantitative detection is vital for chemical industry and environmental monitoring for their toxic effects, so far, very few luminescent sensory systems have been described [14]. The optical sensing of xylenes is possible using Zn(II)-organic frameworks containing fluorescent aromatic moieties such as tetrapyridine tetraphenylethene [14], triazole derivatives [32–34], and tetrakis(4-carboxyphenyl)porphyrin (NUS-40 Zn) [35].

The usage of luminescent MOMs to sense VOCs is promising due to their high stability and ease of preparation, in addition to advantages inherent of the fluorescence technique such as high sensitivity [3,32,36].

Taking this into account, this work is based on the idea that a new metal–organic compound with photoluminescence can be achieved in a single step and in high yield by the straightforward combination of Zn(II) ions with 1,4-benzenedicarboxylic acid and a commercial benzopyridine ligand, which can act as a luminescent unit when coordinated to the metal center. X-ray crystal structures, thermogravimetry, CPMAS ^{13}C-NMR spectroscopy, morphological studies with SEM-EDS, and fluorescent sensing properties obtained for a novel blue luminescent 2D MOF based on Zn-terephthalate with an isoquinoline core are herein discussed.

2. Materials and Methods

2.1. Physical Measurements

All chemicals are commercially available (H_2BDC, 98%; isoquinoline, 98%; and $Zn(NO_3)_2 \cdot 4(H_2O)$, 98% from Sigma-Aldrich (St. Louis, Missouri, United States)) and were used as received. The FT-IR spectrum was recorded in the range of 4000–600 cm^{-1} by using the standard Pike ATR cell on a Bruker Tensor 27 FT-IR spectrophotometer (Bruker Optik GmbH, Ettlingen, Germany). Elemental analysis for C, H, and N were carried out by standard methods using a Vario Micro-Cube analyzer.

Powder X-ray diffraction (PXRD) was conducted using a Bruker D8 ADVANCE X-ray powder diffractometer (Cu-Kα, λ = 1.5418 Å) (Bruker AXS GmbH, Karlsruhe, Germany) with the 2θ range of 5–50°.

Thermogravimetric analyses were performed using TA Instruments equipment, under a dinitrogen atmosphere, at a heating rate of 10 °C min^{-1}, and from 25 to 475 °C.

The CPMAS ^{13}C NMR experiment was recorded with a Bruker Advance II 300 spectrometer (Bruker BioSpin GmbH, Rheinstetten, Germany) (operating at 75 MHz for ^{13}C) on a 4 mm rotor double resonance. The CPMAS experiment was recorded with a contact time of 2 ms and a delay of 5 s at a 7 kHz spinning rate at ambient temperature.

The shape and size of the crystals of compound **1** were examined with scanning electron microscopy (SEM) using a JSM-6510LV microscope from JEOL (JEOL, Ltd, Akishima, Tokyo, Japan) equipped with a Bruker QUANTAX 200 energy-dispersive X-ray spectrometer (EDS) (Bruker Nano GmbH, Adlershof,

Berlin, Germany) for elemental characterization. The crystals were let to dry at room-temperature conditions and fixed on Al stubs with carbon tape and finally coated with a thin layer of gold using a Denton IV sputtering chamber before SEM imaging acquisition.

Luminescence spectra in suspensions of **1** were recorded on an Agilent Cary Eclipse equipped with a crystal holder and a thermostated holder for quartz cuvettes. In all sensing studies, as-synthesized single-crystalline samples of **1** were used. Suspensions of **1** were prepared by stirring for 20 min at 25 °C in spectrophotometric-grade solvents with a final concentration of 25 μM. For the titration experiment of xylenes, a stock suspension of **1** (1 mg mL^{-1}) in acetonitrile was prepared by ultrasonic treatment by 20 min at r.t., and subsequently, 45 μL of this suspension was diluted with 2500 uL of acetonitrile, to give a final concentration of 25 μM, and the emission spectra (λ_{ex} = 330) of the suspension were recorded after adding aliquots of xylenes.

2.2. Synthesis of {[Zn$_2$(μ$_2$-BDC)$_2$(iQ)$_2$]}$_\infty$, **1**

Initially, in a 4 mL vial, 32.6 mg of Zn(NO$_3$)$_2$·4H$_2$O (0.10 mmol) and 15.0 mg of BDC (0.09 mmol) were dissolved with 3 mL of DMF. After two and a half hours, 24 μL (0.20 mmol) of isoquinoline was added using a high-precision micropipette. The solution was stirred for 15 min at 75 °C and was then placed in a Parr bomb and heated at 115 °C for 16 h. After cooling the mixture, colorless crystals were obtained, which were filtered out and washed with DMF. Yield: 82%, based on the metal precursor.

Elemental analysis (%), C$_{34}$H$_{24}$N$_2$O$_8$Zn$_2$, cal.: C, 56.77; H, 3.36, N, 3.89; found: C, 56.72; H, 3.39; N, 3.80. IR (ATR): $\tilde{v}$ 3058 (w), 2087 (w), 1634 (m), 1596 (m), 1586 (m), 1410 (s), 1164 (w), 1041 (w), 1013 (w), 953 (w), 1085 (w), 1051, 861 (w), 823 (s), 732 (s).

2.3. Crystallographic Investigations

The relevant details of the crystal, data collection, and structural refinement can be found in Table 1. Crystallographic data for **1** were collected on a Bruker APEX II CCD diffractometer at 296 K using Mo-K$_\alpha$ radiation (k = 0.71073 Å), from an Incoatec IμS source and Helios optic monochromator [37]. Suitable crystals were coated with hydrocarbon oil (Parabar), and the specimen was collected with a glass fiber and fixed with glue. The structure was solved using intrinsic phasing (SHELXT) [38] and refined by full-matrix least-squares on F2 using the shelXle GUI [39]. The hydrogen atoms of the C–H bonds were placed in idealized positions and their position was refined with U_{iso} linked to the parent atom with distance restraints. Crystallographic data for **1** have been deposited at the Cambridge Crystallographic Data Center (CCDC) with the number 1994765.

Table 1. Crystal data and structure refinement for **1**.

Empirical formula	C$_{34}$ H$_{24}$ N$_2$ O$_8$ Zn$_2$
Formula weight	719.29
Temperature	296(2) K
Wavelength	0.71073 Å
Crystal system	Monoclinic
Space group	P 2/n
Unit cell dimensions	a = 10.9454(4) Å, α = 90°.
	b = 10.9146(4) Å, β = 112.457(2)°.
	c = 13.5283(5) Å, γ = 90°.
Volume	1493.59(10) Å^3
Z	2
Density (calculated)	1.599 mg/m^3
Absorption coefficient	1.664 mm^{-1}
F(000)	732
Crystal size	0.207 x 0.170 x 0.156 mm^3
Theta range for data collection	2.477° to 25.359°.
Index ranges	–13 <= h <= 12, –13 <= k <= 13, –14 <= l <= 16

Table 1. *Cont.*

Reflections collected	12,174
Independent reflections	2730 [R(int) = 0.0264]
Completeness to theta = 25.242°	99.4%
Absorption correction	Analytical
Max. and min. transmission	0.8479 and 0.7915
Refinement method	Full-matrix least-squares on F^2
Data / restraints / parameters	2730 / 216 / 268
Goodness-of-fit on F^2	1.173
Final R indices [I > 2 sigma(I)]	R1 = 0.0529, wR2 = 0.1239
R indices (all data)	R1 = 0.0554, wR2 = 0.1251
Largest diff. peak and hole	1.239 and −1.152 e.Å^{-3}

3. Results and Discussion

3.1. Crystal Structure of {[Zn$_2$(µ$_2$-BDC)$_2$(iQ)$_2$]}$_\infty$, 1

The X-ray crystallographic analysis shows that **1** crystalizes in the monoclinic space group P 2/n, and the asymmetric unit consists of one Zn(II) ion, one BDC dianion, and one isoquinoline molecule (Figure 1). Each Zn(II) ion is five-coordinated in a slightly distorted square pyramidal geometry, coordinated by four carboxyl oxygen atoms of BDC and the nitrogen atom from the isoquinoline molecule. The basal plane is defined by O1, O2, O3, and O4 from four BDC ligands. The apical position is occupied by the nitrogen atom from the coordinated isoquinoline molecule. Toward the apical ligating atom, the metal ion is deviated from the corresponding basal plane by 0.378 Å. The basal planes are found to be very little tetrahedrally distorted with a τ value of 0.012 [τ = (159.01 − 158.29)/60 = 0.012] [40]. The Zn–O bond lengths vary from 2.003(3) to 2.065(4) Å, and the O–Zn–O bond angles range from 88.55(17) to 158.99(17) (Table 2); these values are representative of different coordination geometries of Zn(II) ions in coordination polymers with dicarboxylate-bridging ligands [41–43].
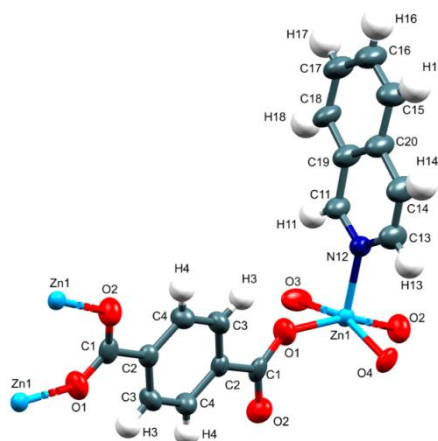

Figure 1. Asymmetric unit of **1**.

In **1**, each BDC ligand bridges four Zn(II) ions, with the two carboxylate moieties assuming a tetrakis(monodentate) coordination mode. As a consequence, pairs of Zn(II) ions are bridged by four carboxylates to form dinuclear secondary building units (SBUs) (Figure 2), which generate a 2D coordination network parallel to the ab plane, enclosing virtually a square grid with a size of 10.945 × 10.915 Å^2. In the SBU, the Zn···Zn distance of 2.9740(11) Å is in the characteristic range of BDC-bridged dinuclear Zn(II) complexes [20,42,44]. Furthermore, a 3D supramolecular network is formed by interpenetrated layers with π–π stacking interactions between the BDC and the secondary ring in the isoquinoline (Figure 3), with a centroid–centroid displacement angle of 7.62° and a distance equal to 3.47(8) Å. Although the presence of the isoquinoline ligand directly attached to the SBU could

contribute to avoiding interpenetration in a similar approach as in the isoreticular series of MOF-2 derivates [45], this phenomenon does not occur in **1**, as the layers along the crystallographic a axis are stabilized by the mentioned π–π interactions.

Table 2. The selected bond lengths (Å) and angles (°) for compound **1**.

Zn(1)-O(4)	2.003(3)	O(4)-Zn(1)-N(12)	102.83(17)
Zn(1)-N(12)	2.033(4)	O(4)-Zn(1)-O(2)#1	88.55(17)
Zn(1)-O(2)#1	2.042(4)	N(12)-Zn(1)-O(2)#1	103.56(17)
Zn(1)-O(3)#2	2.059(4)	O(4)-Zn(1)-O(3)#2	158.30(15)
Zn(1)-O(1)	2.065(4)	O(4)-Zn(1)-O(1)	87.57(17)
Zn(1)-Zn(1)#1	2.9740(11)	N(12)-Zn(1)-O(1)	97.43(17)
		N(12)-Zn(1)-O(3)#2	98.87(17)
		O(2)#1-Zn(1)-O(3)#2	86.9(2)

Symmetry transformations used to generate equivalent atoms: #1 –x + 1/2, y, –z + 5/2; #2 x, y + 1, z.
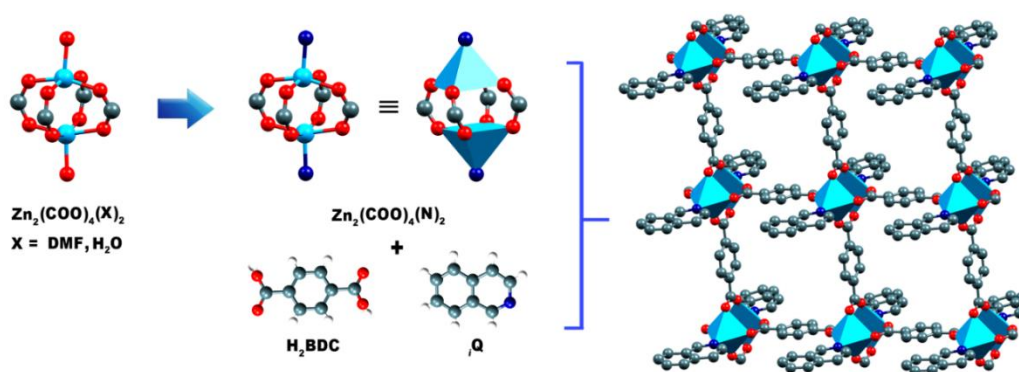
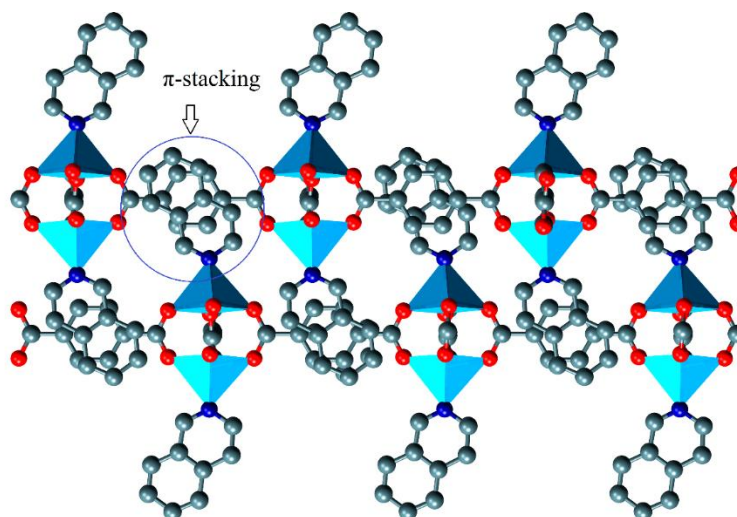**Figure 2.** Dinuclear secondary building unit (SBU) and the 2D coordination array in **1**.

Figure 3. The 3D packing diagram of **1** constructed by π–π stacking interactions.

3.2. PXRD, Thermal Stability, IR-Correlation, and Solid-State Structure-CPMAS ^{13}C NMR Correlation

The purity of the crystalline as-synthesized bulk sample of **1** was examined by powder X-ray diffraction (PXRD) measurements at room temperature (Figure 4). The PXRD patterns of the synthesized sample is consistent with those simulated from single-crystal X-ray data, indicating high phase purity; thus, we used this sample for further solvent sensing studies. The thermal stability of **1** was tested

by thermogravimetric analysis (TGA) under a dinitrogen atmosphere (Figure 5A). Due to the lack of guest solvent molecules, compound **1** presents high stability up to 310 °C. The TGA curve of **1** shows a weight loss of 36.20% from 312 to 411 °C, corresponding to the removal of two coordinated *iQ* molecules (calcd 35.88%). The differential scanning calorimetry curve (DSC) shows a single endotherm peak at 375 °C with $\Delta H = 307$ J/g, which can be attributed to the release of the aromatic N-donor ligand (Figure 5B) [19].
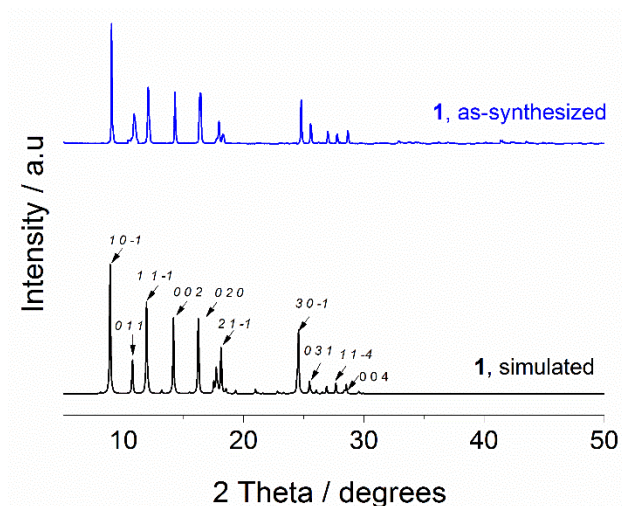
Figure 4. Indexed PXRD simulated pattern and measured pattern of **1** at room temperature.
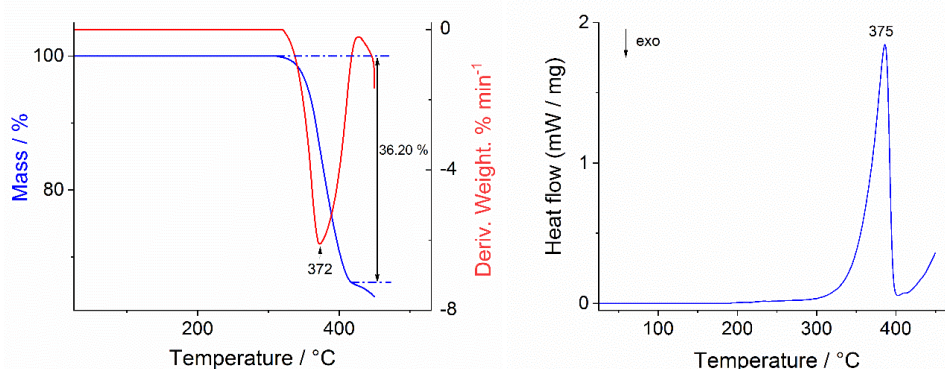
Figure 5. TGA and DTGA curves (**A**) and DSC (**B**) of **1**.

The IR spectrum shows the common bands expected for coordinated carboxylate ligands to atoms Zn(II) along with the corresponding bands to isoquinoline. Two bands of asymmetric and symmetric stretches for the $-CO_2^-$ groups at 1586 and 1410 cm^{-1} and the difference ($\Delta v = 176$ cm^{-1}) can be assigned to the tetrakis(monodentate) coordination mode of the BDC^{2-} ligand, which is in agreement with the crystal structure [46].

The solid-state CPMAS ^{13}C NMR spectrum of **1** (Figure 6) shows three expected signals (red rectangles) for the BDC ligand at 129 and 136 ppm for aromatic carbon atoms (C3 and C4) and the ipso-carbon (C2), respectively, whereas the peak at 171 ppm can be ascribed to the carboxylate (C1) group. All of those assignments are in agreement with the ^{13}C CPMAS NMR spectra of related MOFs such as the zirconio-based MOFs UiO-66 [$Zr_6O_4(OH)_4(BDC)_6$] [47] and MIL-140C [ZrO(BDC)] [47], and zinc-based MOF [$Zn_2(\mu_2\text{-DBC})_2(\mu_4\text{-btre})$] (btre = 1,2-bis(1,2,4-triazol-4-yl)ethane) [48]. The blue rectangles denote the methine signals from the isoquinoline ligand, and, as can be seen, some of those peaks are superimposed along with the BDC signals, especially the ^{13}CH atoms C15, C17, C18, and C19, which are in the range of 127–129 ppm. The two downfield signals at 154 and 141 ppm can be ascribed

to methine groups C11 and C13, respectively. In general, the ^{13}C CPMAS spectrum of **1** is consistent with its crystalline structure.
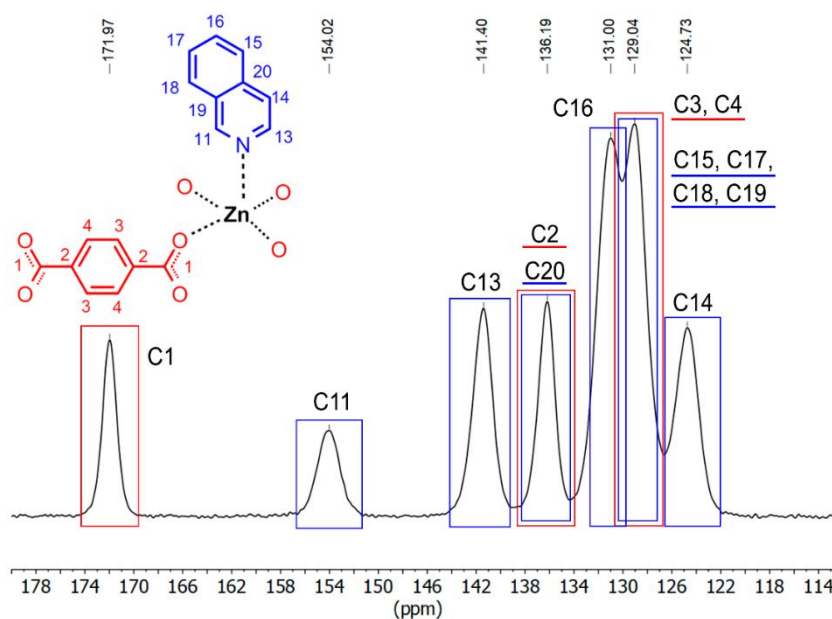

Figure 6. ^{13}C CPMAS NMR spectrum for **1** and numbering scheme of the building unit. Regions with rotation side bands at 8 (16) kHz = 64 (128) ppm from the signal are covered in the NMR spectrum.

3.3. SEM-EDS Analysis

Figure 7 shows SEM micrographs of crystalline compound **1**. Micrometric bars are observed with a well-defined plane facing along the transversal direction. The inset in 7A displays the edge of a bar with the typical cleavage for monoclinic structures (inset 7B), which confirms the crystal system obtained with X-ray diffraction studies. Even though different crystal sizes are shown, the morphology is homogenous, and this could be associated with the presence of only one phase based in the monoclinic unit-cell. EDS elemental mapping of compound **1** is shown in Figure 8. EDS analysis confirms the presence of C, O, and N as part of the chemical composition of the sample; furthermore, it can be observed that the signal of Zn atoms was detected all over the crystals, which can be related to a homogeneous distribution of the Zn in compound **1**.
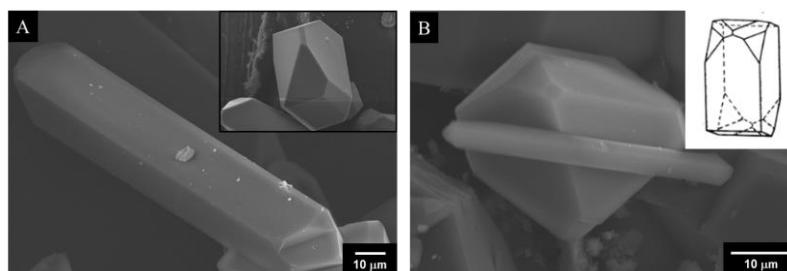

Figure 7. Representative SEM images of compound **1** showing its typical crystal sizes (**A** and **B**, respectively).
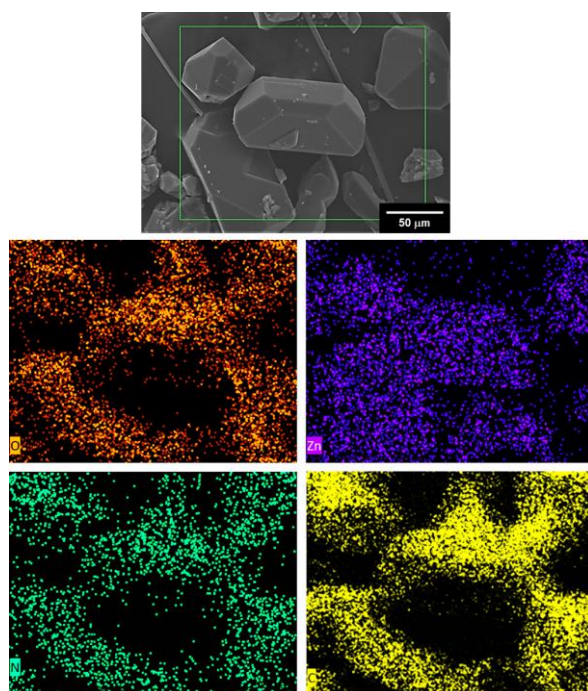
Figure 8. EDS mapping of compound **1**; oxygen (orange), zinc (purple), nitrogen (green), and carbon (yellow).

3.4. Photoluminescent Properties

Currently, luminescent MOMs have been widely studied for sensing different types of small-molecule volatile organic compounds and nitroaromatic compounds [7]; however, the sensing of BTX aromatic solvents (benzene, toluene, xylene isomers) still remains largely unexplored. In order to investigate the potential chemosensing properties of **1**, its photoluminescence spectra of liquid suspensions in several organic solvents including the BTX aromatics, with constant stirring, were analyzed. Figure 9A shows the family of the spectra (λ_{ex} = 330 nm) of **1** (~25 µM). In general, a fluorescence enhancement was observed in the presence of aromatic compounds containing electron-donating groups. Among the studied solvents, p-xylene displays the highest intensity (λ_{em} = 409 nm), followed by m-xylene and o-xylene (λ_{em} = 407 nm). Suspensions in toluene and benzene showed modest emissions at 409 nm, which are significantly lower than that observed for p-xylene. By contrast, alcohols (CH_3OH and EtOH) and aprotic solvents (acetone, $CHCl_3$, CH_3CN, DMF, and THF) practically do not present fluorescent emission. Considering that the acetonitrile suspension does not display emission and this solvent is highly miscible with BTX aromatics, we used an acetonitrile suspension medium of **1** to carry out a solvent sensing experiment due to its potential ability to turn-on fluorescence by addition of xylene isomers, toluene, and benzene. Due to the environmental, chemical, and industrial relevance of xylene isomers, which are anthropogenic polluting solvents, there is growing interest in the development of new luminescent MOF-based sensors in which the analytical responses are based on an increase in fluorescence intensity, rather than quenching, because this limits their practical applications. In this line, the literature features only a few examples for xylene isomer sensing [14,34,35].

Next, the solvent selectivity of an acetonitrile suspension of **1** (~25 µM) was examined by addition of 40 equiv. of BTX, and an emission intensity increase at 409 nm was recorded. Benzene and toluene gave low responses (Figure 9B). Interestingly, **1** showed sensitivity to xylene isomers, especially p-xylene with a considerable increase in its blue emission (I_F/I_0 = 27.2), as shown in Figure 9B. The differing "turn-on" response of the methyl-substituted aromatic VOCs versus the polar aprotic solvents demonstrates the potential of this material to act as a selective and sensitive sensor, and a

potential π–π interaction may arise as a mechanism of interaction between **1** and BTX, which depends on the electro-donating ability of the substituents, as shown in Figure 9B. This fluorescent enhancement may be related to the different interactions between compound **1** and xylene isomers, which have different shapes and volumes; thus, p-xylene is linear and can easily present π–π interactions with the isoquinoline fragments groups. A PLATON program analysis shows that there is about 5% of the crystal volume accessible to solvents [49], which is very limited.
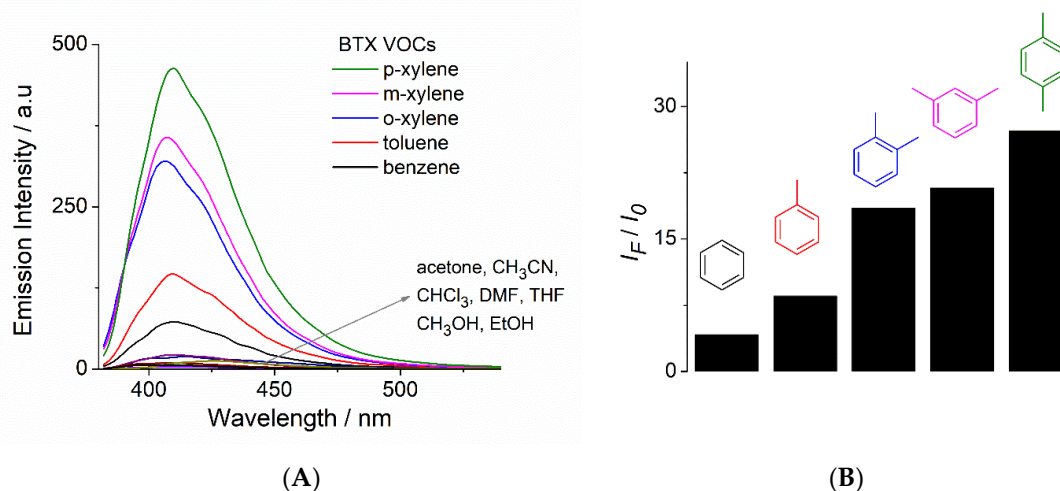

(A)   (B)

Figure 9. (**A**) Emission spectra of **1** (λ_{ex} = 330 nm) at room temperature in different pure organic solvents and (**B**) fluorescence intensity changes at 409 nm (λ_{ex} = 330 nm) of acetonitrile suspension of **1** upon addition of 40.0 equiv. of benzene, toluene, xylene isomers (BTX).

It is well-known that the fluorescent emission of MOFs is strongly dependent on their chemical environment such as solvation, which can change the relative contributions of charge transfers and intraligand luminescence [2,7]. The weak fluorescence or null of **1** in suspensions of polar solvents such as water, alcohols, and DMF is not unexpected, because these solvents are among the most efficient vibrational quenchers [7]. On the other hand, solvation with hydrophobic aromatic molecules can favor charge transfer processes, which results in an increase in fluorescence.

A similar "turn-on" response has been reported for some MOF-based sensors, and this has been ascribed to an aggregation-enhanced emission [14].

In order to estimate the sensitivity of **1** to p-xylene, a fluorescence titration experiment was carried out by addition of increasing amounts of this solvent to an acetonitrile suspension of **1**. The addition of p-xylene (0–40 equiv.) induced a turn-on fluorescence response (Figure 10). For the concentration range of [p-xylene] <200 μM, the emission shows a linear dependence, as shown in Figure 10 (inset). The detection limit (LOD) of p-xylene for **1**, defined as LOD = 3σ/s, where σ is the standard deviation of the blank signals and s is the slope of the calibration curve with the linear fit (inset, Figure 10), is 10 ± 0.3 μM.

Finally, in order to explore the chemical stability of **1** and potential guest introduction inside the layers, we compared PXRD patterns and FTIR spectra of the as-synthesized compound **1** and a sample of this MOF treated with p-xylene by stirring (30 min) at r.t. In general, the patterns and IR spectra are very similar to each other (Figure 11), before and after treatment, indicating that its crystal structure remains intact in the presence of p-xylene. This chemical stability can be favored by very limited access to solvents. In this sense, the enhancement of fluorescence can be mainly attributed to the solvation phenomenon.
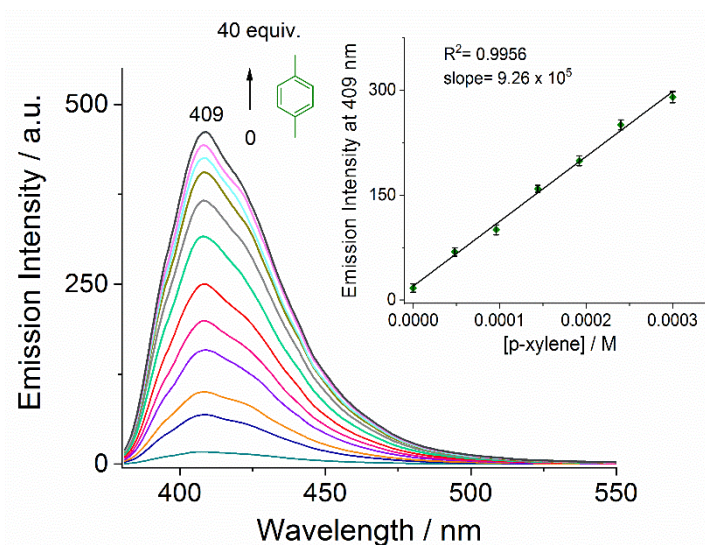
Figure 10. Changes in the emission spectra (λ_{ex} = 330 nm) of acetonitrile suspension of **1** upon addition of increasing amounts of p-xylene (0–300 μM). The inset shows the calibration curve with a linear fit at λ_{em} = 409 nm (average of triplicate experiments).

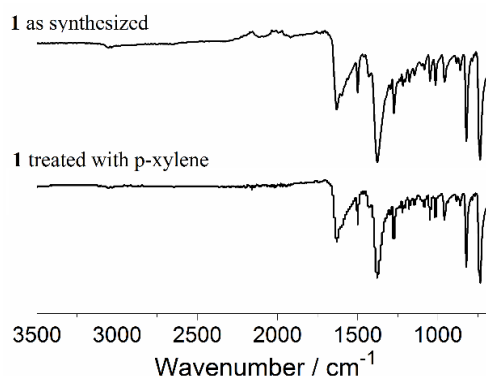**Figure 11.** IR-ATR (attenuated total reflection) of as-synthesized **1** and treated with p-xylene isomer.

4. Conclusions

A new Zn(II)-based metal−organic framework, **1**, has been designed and synthesized by solvothermal synthesis combining terephthalic acid and isoquinoline in DMF. X-ray crystallographic studies revealed interpenetrated 2D networks containing a dinuclear Zn_2 paddle-wheel core. Photoluminescence properties of **1** in suspensions of xylene isomers show that **1** possesses a strong blue emission with a maximum at 409 nm. Compound **1**, suspended in acetonitrile, can be used as a luminescent material for the sensing of p-xylene in the micromolar concentration range based on an increase in its fluorescent emission.

The strong emission of **1** in combination with the straightforward synthesis and its high thermal stability up to 310 °C makes it a promising candidate for the design of more sophisticated blue-light-emitting materials with potential application in sensing of methyl-substituted aromatic VOCs.

Author Contributions: L.D.R.-V. and I.J.B.R. Synthesized and performed the experiments; S.H.-O. Single-crystal X-ray diffraction; A.R.V.-N. SEM-EDS analysis; J.d.J.C.-M. Contributed reagents and analysis of data; A.D.-G. and V.S.-M. wrote the paper. All authors have read and agreed to the published version of the manuscript.

References

1. Lei, J.; Qian, R.; Ling, P.; Cui, L.; Ju, H. Design and sensing applications of metal-organic framework composites. *Trends. Anal. Chem.* **2014**, *58*, 71–78. [CrossRef]

2. Allendorf, M.D.; Bauer, C.A.; Bhakta, R.K.; Houk, R.J.T. Luminescent metal-organic frameworks. *Chem. Soc. Rev.* **2009**, *38*, 1330–1352. [CrossRef] [PubMed]

3. Kreno, L.E.; Leong, K.; Farha, O.K.; Allendorf, M.D.; Van Duyne, R.P.; Hupp, J.T. Metal-organic framework materials as chemical sensors. *Chem. Rev.* **2012**, *112*, 1105–1125. [CrossRef] [PubMed]

4. Liao, Z.; Xia, T.; Yu, E.; Cui, Y. Luminescent metal–organic framework thin films: From preparation to biomedical sensing applications. *Crystals.* **2018**, *8*, 338. [CrossRef]

5. Zhang, X.; Wang, W.; Hu, Z.; Wang, G.; Uvdal, K. Coordination polymers for energy transfer: Preparations, properties, sensing applications, and perspectives. *Coord. Chem. Rev.* **2015**, *284*, 206–235. [CrossRef]

6. Zhang, N.; Guan, Q.L.; Liu, C.H.; Sun, Y.; Li, B.; Xing, Y.H.; Bai, F.Y. A rht-Type Luminescent Zn (II)-MOF Constructed by Triazine Hexacarboxylate Ligand: Tunable Luminescent Performance and White-light Emission Regulation through doping Eu^{3+}/Tb^{3+}. *Appl. Organometal Chem.* **2020**, *34*, 1–10. [CrossRef]

7. Müller-Buschbaum, K.; Beuerle, F.; Feldmann, C. MOF based luminescence tuning and chemical/physical sensing. *Microporous Mesoporous Mater.* **2014**, *216*, 171–199. [CrossRef]

8. Kumar, P.; Deep, A.; Kim, K.; Brown, R.J.C. Progress in Polymer Science Coordination polymers: Opportunities and challenges for monitoring volatile organic compounds. *Prog. Polym. Sci.* **2015**, *45*, 102–118. [CrossRef]

9. Rosales-Vázquez, L.D.; Valdes-García, J.; Bazany-Rodríguez, I.J.; Germán-Acacio, J.M.; Martínez-Otero, D.; Vilchis-Néstor, A.R.; Morales-Luckie, R.; Sánchez-Mendieta, V.; Dorazco-González, A. A sensitive photoluminescent chemosensor for cyanide in water based on a zinc coordination polymer bearing ditert-butyl-bipyridine. *Dalt. Trans.* **2019**, *48*, 12407–12420. [CrossRef]

10. Wu, S.; Lin, Y.; Liu, J.; Shi, W.; Yang, G.; Cheng, P. Rapid Detection of the Biomarkers for Carcinoid Tumors by a Water Stable Luminescent Lanthanide Metal–Organic Framework Sensor. *Adv. Funct. Mater.* **2018**, *28*, 1–10. [CrossRef]

11. Pramanik, S.; Zheng, C.; Zhang, X.; Emge, T.J.; Li, J. New Microporous Metal–Organic Framework Demonstrating Unique. *J. Am. Chem. Soc.* **2011**, *133*, 4153–4155. [CrossRef] [PubMed]

12. Zhang, L.; Kang, Z.; Xin, X.; Sun, D. Metal–Organic frameworks based luminescent materials for nitroaromatics sensing. *CrystEngComm* **2015**. *18*, 193–206. [CrossRef]

13. Rosales-Vázquez, L.D.; Sánchez-Mendieta, V.; Dorazco-González, A.; Martínez-Otero, D.; García-Orozco, I.; Morales-Luckie, R. Cadmium-1,4-cyclohexanedicarboxylato coordination polymers bearing different di-alkyl-2,2'-bipyridines: Syntheses, crystal structures and photoluminescence studies. *Dalt. Trans.* **2017**, *46*, 12516–12526. [CrossRef] [PubMed]

14. Jackson, S.L.; Rananaware, A.; Rix, C.; Bhosale, S.V.; Latham, K. Highly Fluorescent Metal-Organic Framework for the Sensing of Volatile Organic Compounds. *Cryst. Growth Des.* **2016**, *16*, 3067–3071. [CrossRef]

15. Kumar, P.; Deep, A.; Kim, K.-H. Metal organic frameworks for sensing applications. *Trends. Anal. Chem.* **2015**, *73*, 39–53. [CrossRef]

16. Zhou, J.M.; Shi, W.; Xu, N.; Cheng, P. Highly selective luminescent sensing of fluoride and organic small-molecule pollutants based on novel lanthanide metal-organic frameworks. *Inorg. Chem.* **2013**, *52*, 8082–8090. [CrossRef] [PubMed]

17. Wang, X.; Qin, C.; Wang, E.; Li, Y.; Hao, N.; Hu, C.; Xu, L. Syntheses, structures, and photoluminescence of a novel class of d^{10} metal complexes constructed from pyridine-3,4-dicarboxylic acid with different coordination architectures. *Inorg. Chem.* **2004**, *43*, 1850–1856. [CrossRef]

18. Liu, G.X.; Zhu, K.; Chen, H.; Huang, R.Y.; Xu, H.; Ren, X.M. Two novel three-dimensional coordination polymers based on metal clusters: Hydrothermal syntheses, crystal structures and luminescence. *Inorg. Chim. Acta* **2009**, *362*, 1605–1610. [CrossRef]

19. Rendón-Balboa, J.C.; Villanueva-Sánchez, L.; Rosales-Vázquez, L.D.; Valdes-García, J.; Vilchis-Nestor, A.R.; Martínez-Otero, D.; Martínez-Vargas, S.; Dorazco-González, A. Structure of a luminescent 3D coordination polymer constructed with a trinuclear core of cadmium-trimesate and isoquinoline. *Inorg. Chim. Acta* **2018**, *483*, 235–240. [CrossRef]

20. Ma, B.Q.; Mulfort, K.L.; Hupp, J.T. Microporous pillared paddle-wheel frameworks based on mixed-ligand coordination of zinc ions. *Inorg. Chem.* **2005**, *44*, 4912–4914. [CrossRef] [PubMed]

21. Li, M.; Li, D.; O'Keeffe, M.; Yaghi, O.M. Topological analysis of metal-organic frameworks with polytopic linkers and/or multiple building units and the minimal transitivity principle. *Chem. Rev.* **2014**, *114*, 1343–1370. [CrossRef]

22. Munn, A.S.; Amabilino, S.; Stevens, T.W.; Daniels, L.M.; Clarkson, G.J.; Millange, F.; Lennox, M.J.; Düren, T.; Bourelly, S.; Llewellyn, P.L.; et al. Metal-organic frameworks from divalent metals and 1,4-benzenedicarboxylate with bidentate pyridine-N-oxide co-ligands. *Cryst. Growth Des.* **2015**, *15*, 891–899. [CrossRef]

23. Hawxwell, S.M.; Brammer, L. Two-dimensional metal-organic frameworks containing linear dicarboxylates. *Acta Cryst. Sect. B Struct. Sci.* **2006**, *3*, 808–814. [CrossRef]

24. Luisi, B.S.; Ma, E.Z.; Moulton, E.B. Tri-metal Secondary Building Units: Toward the Design of Thermally Robust Crystalline Coordination Polymers. *J. Chem. Crystallogr.* **2007**, *37*, 743–747. [CrossRef]

25. Hailian, L.; Eddaoudi, M.; Groy, T.L.; Yaghi, O.M. Establishing Microporosity in Open Metal–Organic Frameworks: Gas Sorption Isotherms for Zn (BDC). *J. Am Chem Soc.* **1998**, *120*, 8571–8572.

26. Tao, J.; Tong, M.-L.; Shi, J.-X.; Chen, X.-M.; Ng, S.W. Blue photoluminescent Zinc coordination polymers with supertetranuclear cores. *Chem. Commun.* **2000**, *20*, 2043–2044. [CrossRef]

27. Mirzaei, A.; Kim, J.H.; Kim, H.W.; Kim, S.S. Resistive-based gas sensors for detection of benzene, toluene and xylene (BTX) gases: A review. *J. Mater. Chem. C.* **2018**, *6*, 4342. [CrossRef]

28. Martins, V.D.; Granato, M.A.; Rodrigues, A.E. Isobaric Vapor-Liquid Equilibrium for Binary Systems 2,2,4-Trimethylpentane with o-Xylene, m-Xylene, p-Xylene, and Ethylbenzene at 250 kPa. *J. Chem. Eng. Data* **2014**, *59*, 1499. [CrossRef]

29. Rushi, A.D.; Datta, K.P.; Ghosh, P.S.; Mulchandani, A.; Shirsat, M.D. Selective Discrimination among Benzene, Toluene, and Xylene: Probing Metalloporphyrin-Functionalized Single-Walled Carbon Nanotube-Based Field Effect Transistors. *J. Phys. Chem. C.* **2014**, *118*, 24034. [CrossRef]

30. Liu, F.F.; Escher, B.I.; Were, S.; Duffy, L.; Ng, J.C. Mixture effects of benzene, toluene, ethylbenzene, and xylenes (BTEX) on lung carcinoma cells via a hanging drop air exposure system. *Chem. Res. Toxicol.* **2014**, *27*, 952–959. [CrossRef]

31. WHO (1993) Benzene, in Environmental Health Criteria 150, World Health Organization, International. Program on Chemical Safety. Available online: http://www.inchem.org/documents/ehc/ehc/ehc150.htm (accessed on 6 April 2020).

32. Pamei, M.; Puzari, A. Luminescent transition metal–organic frameworks: An emerging sensor for detecting biologically essential metal ions. *Nano-Struct. Nano-Objects.* **2019**, *19*, 100364. [CrossRef]

33. Zhang, J.; Zhang, X.; Chen, J.; Deng, C.; Xu, N.; Shi, W.; Chen, P. Highly selective luminescent sensing of xylene isomers by a water stable Zn-organic framework. *Inorg. Chem. Commun.* **2016**, *69*, 1–3. [CrossRef]

34. Semitut, E.Y.; Sukhikh, T.S.; Filatov, E.Y.; Anosova, G.A.; Ryadun, A.A.; Kovalenko, K.A.; Potapov, A.S. Synthesis, crystal structure, and luminescent properties of novel zinc metal-organic frameworks based on 1,3-Bis(1,2,4-triazol-1-yl)propane. *Cryst. Growth Des.* **2017**, *17*, 5559–5567. [CrossRef]

35. Zhang, J.; Wang, J.; Long, S.; Peh, B.; Dong, J.; Wang, Y.; Karmakar, A.; Yuan, Y.D.; Cheng, Y.; Zhao, D. Luminescent Metal-Organic Frameworks for the Detection and Discrimination of o-Xylene from Xylene Isomers. *Inorg. Chem.* **2018**, *57*, 13631–13639. [CrossRef] [PubMed]

36. Zhang, H.; Ma, J.; Chen, D.; Zhou, J.; Zhang, S.; Shia, W.; Cheng, P. Microporous heterometal-organic framework as a sensor for BTEX with high selectivity. *J. Mater. Chem. A.* **2014**, *2*, 20450–20453. [CrossRef]

37. *APEX 2 Software Suite*; Bruker AXS Inc.: Madison, WI, USA, 2010.

38. Sheldrick, M.G. SHELXT–Integrated space-group and crystal-structure determination . *Acta Crystallogr. Sect. A Found. Adv.* **2015**, *A71*, 3. [CrossRef]

39. Hübschle, B.C.; Sheldrick, G.M.; Dittrich, B. ShelXle: A Qt graphical user interface for SHELXL. *J. Appl. Crystallogr.* **2011**, *44*, 1281. [CrossRef]

40. Addison, A.W.; Rao, T.N.; Reedijk, J.; van Rijn, J.; Verschoor, G.C. Synthesis, Structure, and Spectroscopic Properties of copper(II) compounds containing nitrogen–sulphur donor ligands; the crystal and molecular structure of aqua[1,7-bis(N-methylbenzimidazol-2′-yl)-2,6-dithiaheptane]copper(II) perchlorate. *J. Chem. Soc. Dalton. Trans.* **1984**, *1*, 1349–1356. [CrossRef]

41. Chisca, D.; Croitor, L.; Petuhov, O.; Kulikova, O.V.; Galina, F.; Volodina, G.F.; Coropceanu, E.B.; Masunov, A.E.; Fonari, M.S. Tuning structures and emissive properties in a series of Zn(II) and Cd(II) coordination polymers containing dicarboxylic acids and nicotinamide pillars. *CrystEngComm* **2018**, *20*, 432–447. [CrossRef]

42. Cui, K.; Ma, J.; Huo, X.K.; Qu, Z.; Zhang, J.X. A new 2D Zinc(II)-organic framework with dinuclear units based on iodinated terephthalate: Synthesis, crystal structure and luminescence behavior. *Z. Fur Nat. Sect. B. J. Chem. Sci.* **2014**, *69*, 859–863. [CrossRef]

43. Shi, Z.; Pan, Z.; Jia, H.; Chen, S.; Qin, L.; Zheng, H. Zn(II)/Cd(II) terephthalate coordination polymers incorporating Bi-, Tri-, and tetratopic phenylamine derivatives: Crystal structures and photoluminescent properties. *Cryst. Growth Des.* **2016**, *16*, 2747–2755. [CrossRef]

44. Wang, F.K.; Yang, S.Y.; Huang, R.B.; Zheng, L.S.; Batten, S.R. Control of the topologies and packing modes of three 2D coordination polymers through variation of the solvent ratio of a binary solvent mixture. *CrystEngComm* **2008**, *10*, 1211–1215. [CrossRef]

45. Schoedel, A.; Yaghi, O.M. Porosity in Metal–Organic Compounds. In *Macrocyclic and Supramolecular Chemistry How Izatt–Christensen Award Winners Shaped the Field*; Reed, M.I., Ed.; John Wiley & Sons Inc: Chichester, West Sussex, UK, 2016; Volume 1, pp. 210–212.

46. Dorazco-González, A.; Martinez-Vargas, S.; Hernández-Ortega, S.; Valdés-Martínez, J. Directed self-assembly of mono and dinuclear copper(II) isophthalates into 1D polymeric structures. Design and an unusual cocrystallization. *CrystEngComm* **2013**, *15*, 5961–5968.

47. Bennett, T.D.; Todorova, T.K.; Baxter, E.F.; Reid, D.G.; Gervais, C.; Bueken, B.; Van de Voorde, B.; De Vos, D.; Keenf, D.A.; Mellot-Draznieks, C. Connecting defects and amorphization in UiO-66 and MIL-140 metal-organic frameworks: A combined experimental and computational study. *Phys. Chem. Chem. Phys.* **2016**, *18*, 2192–2201. [CrossRef] [PubMed]

48. Habib, H.A.; Hoffmann, A.; Höppe, H.A.; Janiak, C. Crystal structures and solid-state CPMAS ^{13}C NMR correlations in luminescent zinc(II) and cadmium(II) mixed-ligand coordination polymers constructed from 1,2-bis(1,2,4-triazol-4-yl)ethane and benzenedicarboxylate. *Dalt. Trans.* **2009**, *10*, 1742–1751. [CrossRef] [PubMed]

49. Spek, A.J. Single-crystal structure validation with the program. *PLATON J. Appl. Crystallogr.* **2003**, *36*, 7. [CrossRef]